VIIRS reflective solar bands on-orbit calibration using solar diffuser illuminated by scattered light through the nadir-port

JUNQIANG SUN,[1,2,*] MIKE CHU,[1,3] MENGHUA WANG[1]

[1]*NOAA National Environmental Satellite, Data, and Information Service Center for Satellite Applications and Research E/RA3, 5830 University Research Ct., College Park, MD 20740, USA*
[2]*Global Science and Technology, 7855 Walker Drive, Suite 200, MD 20770, USA*
[3]*Cooperative Institute for Research in the Atmosphere, Colorado State University, Fort Collins, CO 80523, USA*
**Corresponding author: junqiang.sun@noaa.gov*

Received XX Month XXXX; revised XX Month, XXXX; accepted XX Month XXXX; posted XX Month XXXX (Doc. ID XXXXX); published XX Month XXXX

A new variant to the standard on-orbit calibration of the reflective solar bands (RSBs) using a solar diffuser (SD) is formulated. Instead of direct solar exposure through the SD port in the front of instrument as originally designed, the variant method uses light reflecting off Earth's surface coming through the nadir port as the light source to illuminate the built-in onboard SD. The methodology is applied to the Visible Infrared Imaging Radiometer Suite (VIIRS) on board the Suomi National Polar-orbiting Partnership (SNPP) satellite, and is shown to be viable and useful. This approach effectively preserves the standard calibration pipeline other than using a different set of illumination data, corresponding to a different illumination source, for computing the luminosity emanating from the SD. It has the added advantages of not dealing with operational needs for the standard calibration activities and completely bypassing the characterization of the transmission function of the attenuation screen in the front of the SD port. The RSB calibration coefficients are computed from the data of scattered light from the SD sector per each orbit and a sixteen-day average is taken. The variant calibration coefficients are shown to well match the standard solar-based RSB calibration coefficients for all RSBs studied. The result also shows a consistent 2% variation mission-long for all RSBs, showing the overall consistency of this first analysis of the new method but also the level of the uncertainty. The result and the implications of this study are discussed.

OCIS codes: *(280.0280) Remote sensing and sensors; (120.0120) Instrumentation, measurement, and metrology; (010.0010) Atmospheric and oceanic optics.*

http://dx.doi.org/10.1364/AO.99.099999

1. INTRODUCTION

The on-orbit calibration for many satellite sensors is of fundamental importance in making accurate Earth observations from which reliable science products are generated. In the past two decades, the reflective solar bands (RSBs), which operates between 400 nm and 2200 nm in the radiative regime, have seen their full and proven calibration made possible by the use of a specially made panel with nearly ideal diffusive reflectance, commonly referred to as the solar diffuser (SD), as an integral part of on-orbit calibration strategy. The twin MODerate-resolution Imaging Spectroradiometer (MODIS) on-board the Terra and Aqua spacecrafts were the first to be equipped with a full suite of onboard calibrators (OBCs) [1,2] that carries out regularly scheduled inflight monitoring and calibration measurements [3,4]. In the OBC suites for the twin MODIS are the specially manufactured SD made of Spectralon for the calibration of the RSBs [5,6]. The Visible Infrared Imaging Radiometer Suite (VIIRS) on-board Suomi National Polar-orbiting Partnership (SNPP), followed suit with nearly matching layout for its OBC suite [7-9], also is equipped with a Spectralon-made SD for the on-orbit calibration of its RSBs [10-13]. For these three legacy instruments, the calibration of the RSBs relies on the accurate calculation of the RSB sensor response to quantifiable amount of direct solar illumination [13] that reflects off the SD. Numerous newer follow-on sensors will follow a very similar on-orbit calibration strategy utilizing some specially made diffuser panel. This includes the Sentinel-3 Ocean and Land Colour Instrument (OLCI) [14] recently launched on 16 February 2016 and JPSS J1 – J4 VIIRS [15] that are to come. It is clear that the coming era of Earth observations and science products associated with RSBs remains reliant upon the SD-based calibration methodology. Further improvements and progress made to the current operational methodology therefore will be highly beneficial. For this purpose, this work explores a variant method of the SD-based calibration that has potential for future applications as an official method as well as a long-term monitoring tool.

In the current operational procedure for SNPP VIIRS, the on-orbit RSB calibration using the SD occurs during a short time interval when the sensor crosses the terminator, during which the SD is fully illuminated by direct solar exposure through the SD port [13]. The direct sunlight diffusively reflects off the SD for which a quantifiable amount of light reaches the RSB. The RSB response to the known amount of light then is used to characterize the RSB performance and to derive the calibration coefficient [12,13]. It is noted here that the reflectance of the SD is a key input into the RSB performance characterization needed to quantify the amount of light registered by the RSBs. Because the performance of the SD degrades on-orbit, a solar diffuser stability monitor (SDSM), a part of the OBC suite, is used to regularly monitor the SD reflectance performance [16-18].

The current official on-orbit calibration strategy using solar illumination for the SD comes with numerous challenges. On a general level, the current approach is somewhat restrictive involving numerous complex components and demanding rigorous efforts that include pre-launch analyses [18], characterization of known optical effects and continual analyses and monitoring. For example, among the numerous additional considerations and add-ons that increase the complexity of the calibration procedure, one such complication is the attenuation screen placed in front of the SD port for the purpose of preventing detector saturation of high response bands. This added screen tags on an additional optical effect, the vignetting effect coming from the pinholes of the screen, that also must be correctly characterized. This characterization of the transmission function of the screen is known as the vignetting function (VF). It is well known that residual error of VF from poor characterization leads to significant seasonally patterned artifacts on the order of a few percent [19,20] that will impact the accuracy of the science products. Another issue is the proper selection of the full illumination interval of the data, called "sweet spot", of the detector response that can be used for performance characterization. Sun and Wang [13,16] have already discussed an improved selection of the sweet spots different from the standard operational procedure.

Although the current official calibration approach is complex and restrictive, the procedure and the instrument design nevertheless permit some flexibility for alternative considerations. For example, a Moon-based RSB calibration methodology [21-24], for which the spacecraft performs a special maneuver to align the SV port toward the Moon for lunar observation [25], now is an established approach. The result of the lunar calibration is also already implemented for twin MODIS [22] and SNPP VIIRS [23, 24] as an integral part of the current on-orbit RSB calibration to improve upon the operational methodology. It is worth emphasizing that different calibration strategies, such as ones mentioned above, are valuable alternatives to improve upon the operational approach. This paper presents one such viable variant of the SD-based on-orbit RSB calibration using light scattered off the Earth's surface coming through the nadir port as the illumination source. The new variant has numerous obvious advantages over the operational procedure that uses full solar-illumination. First and foremost, the variant takes full advantage of scattered light through the nadir port which naturally occurs during the daytime portion of the flight, thus bypassing any scheduling or operational demands for RSB calibration. Second, by using light through the nadir port, the variant circumvents the complication associated with the attenuation screen and its characterization. Additional simplifications and other advantages, including no saturation for bands of higher response, make this new approach easier and more flexible to implement.

One associated issue of potential interest pertains to the recently discovered "SD degradation nonuniformity (SDDNU) effect" [26]. This refers to a non-ideal anisotropic behavior in the degradation of the SD that is contrary to the assumed conditions in the official procedure. It has been shown that both SNPP VIIRS and MODIS suffer this nonuniformity effect [26] in the SD degradation that is a significant progenitor of the inherent RSB calibration error due to the fact that the standard methodology does not account for this effect. While the reason for the RSB calibration error in twin MODIS was unknown at the time of the development of the MODIS Collection 6 methodology, Sun et al. have developed a different calibration strategy for MODIS using Earth targets to improve RSB calibration accuracy [27,28]. For SNPP VIIRS, the mitigation of this error relies on using lunar calibration result to reset the long-term calibration baseline [29,30]. This RSB calibration error stemming from the SD is a result of the difference between the outgoing angles of SD to the SDSM versus that of SD to the RSBs. As it is now well established that the reflectance of SD does not maintain the same angular dependence along with its overall performance degradation on orbit [26] with respect to the outgoing angle, this variant approach may provide different insight into this effect by also examining the potential impact of different incident angles.

The paper is organized as follows. Section 2 briefly describes the illumination of SD and its usability in both the standard operational procedure and the new variant approach. Section 3 lays out the formalism and the data analysis procedure for the RSB calibration using Earth-scattered light. Section 4 presents the result of the variant approach and shows comparison with the standard result. Section 5 discussions several key and related issues. Section 6 summarizes and concludes.

2. ILLUMINATION OF SD AND SD OBSERVATION RSB RESPONSE

For SNPP VIIRS, its SD, as shown in Fig. 1, is installed in the instrument chamber as a component of a full OBC suite [5, 13]. It is a particular make of diffuser panel made of Spectralon that has already been deployed for older sensors including the twin MODIS [3, 4].

Fig. 1. A solar diffuser.

The SNPP satellite flies at a geosynchronous orbit with inclination at 98.7° at an altitude of 834 km that makes a complete orbit once every 101 minutes [9-11]. The schematic in Fig. 2 illustrates the flight path of SNPP VIIRS showing the part of the flight path when the satellite and the instrument approach the terminator from the night side where onboard calibration occurs [25]. Data acquisition for the operational RSB calibration is carried out during this short time interval of terminator crossing when the SV port and the SD align in the direction of the Sun for the full illumination of the SD [13].

In the short interval before the terminator crossing, the light comes through the SD port and reflects off the SD to reach the Rotating Telescope Assembly (RTA), which directs the light to the RSBs, and the SDSM. This is illustrated in Fig. 3. Although terminator crossing occurs

every orbit, the characterization of the SD reflectance via SDSM measurements is operated only at scheduled times that are typically a few days apart. The characterization of the RSBs, however, can be and is performed every orbit since the SV port is permanently open without any protective SD door and the RSB sensors remain operational. Figure 3 also illustrates the illumination coming from the Earth-scattered light through the nadir port, reaching the SD at an incident angle different from that of solar illumination. The direction to the nadir port from the SD nominally points downward into the plane of the schematic.

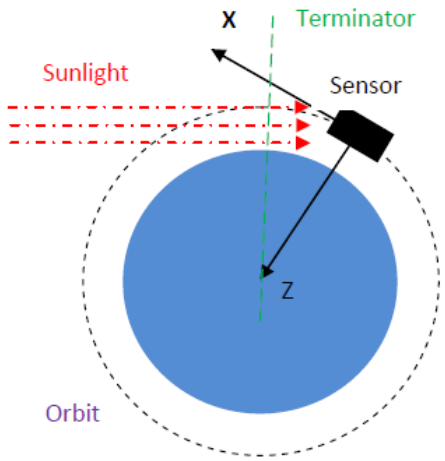

Fig. 2. Schematic of on-orbit SD/SDSM calibration and flight path of SNPP VIIRS.

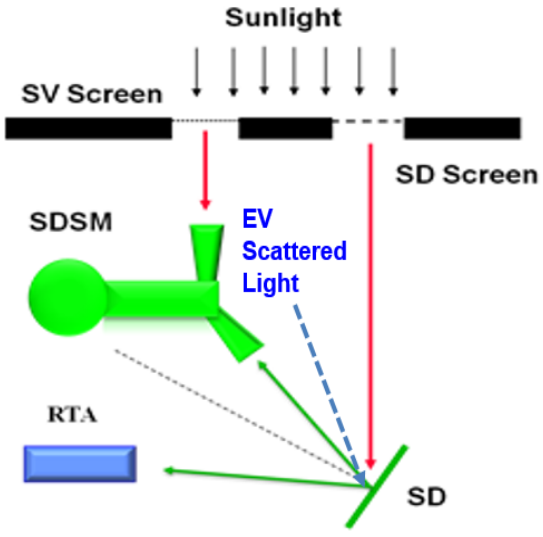

Fig. 3. Schematic of on-orbit SD/SDSM calibration and flight path of SNPP VIIRS.

In reality the illumination of the SD continues throughout the entire dayside part of the flight beyond full solar illumination. Figure 4 shows an example response curve to the light coming from the SD sector registered by band M1 detector 1 for high gain, over the entire daytime half of an orbit. The signals are expressed in the output of the detector reading as digital count (dn). The flight path corresponds to the decreasing of declination angle, as defined in the instrument coordinate system, from right to left as shown in the plot, beginning near the time interval when the SNPP is about to cross the terminator from the night-side near 0° declination. The top plateau of the large peak on the right side of the plot near 0° declination corresponds to the band M1 detector's response to the full illumination of the SD just before terminator crossing, as illustrated in Fig. 2. The two sides of the peak correspond to the partial illumination of the SD that quickly rises or drops as the SD enters or leaves the illumination phase. As the instrument moves across the terminator and into the daytime part of the flight, band M1 detector 1 continues to register non-zero signals, shown as the low signals in Fig. 4 to the left side of the vertical dashed line.

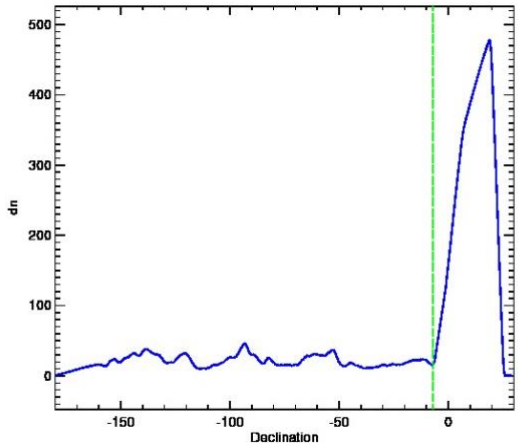

Fig. 4. SD view response of SNPP VIIRS band M1 detector 1 for high gain.

Table 1. VIIRS RSB and SDSM Specification

SDSD Detector	CW* (nm)	VIIRS Band	CW* (nm)	Band Gain
D1	412	M1	410	DG
D2	450	M2	443	DG
D3	488	M3	486	DG
D4	555	M4	551	DG
NA	NA	I1	640	SG
D5	672	M5	671	DG
D6	746	M6	745	SG
D7	865	M7	862	DG
D7	865	I2	862	SG
D8	935	NA	NA	NA
NA	NA	M8	1238	SG
NA	NA	M9	1378	SG
NA	NA	M10	1610	SG
NA	NA	I3	1610	SG
NA	NA	M11	2250	SG

*CW: Center Wavelength; DG: Dual Gain; SG: Singla Gain

The pattern of illumination is similar for all other RSBs. VIIRS has 14 RSBs, three images bands I1-I3 and 11 image bands M1-M11. Among these bands, eight bands are single gain bands while other six are dual gain bands. The center wavelengths of the RSBs and their gains are listed in Table 1. Since the on-orbit SD degradation is tracked by the onboard SDSM, the wavelengths of the SDSM detectors are also listed in Table 1. Detectors of all single gain bands have similar SD view response profile as shown in Fig. 4. For a dual gain band, its gain status switches from high gain to low gain and then low gain to high gain in a four-scan cycle, continuously staying in one gain status for two scans and then jumping to other. Figures 4 only shows the SD view response of band

M1 detector 1 for high gain. The profile for low gain of the detector is similar as for high gain shown in Fig. 4 but with a smaller magnitude. For a detector of a single gain band, there is only one profile of the SD view response, similar as that shown in Fig. 4.

For operational RSB calibration, only a selected interval within the full solar illumination stage called the "sweet spot" is used. Figure 5 shows the "sweet spot" of band M1 detector 1 marked by the two vertical dash lines within the full illumination interval. The full illumination interval corresponds to the large peak in Fig. 4 and flight position illustrated in Fig. 2. The acquired data in the "sweet spot" are used to compute the standard F-factor following the official operational procedure.

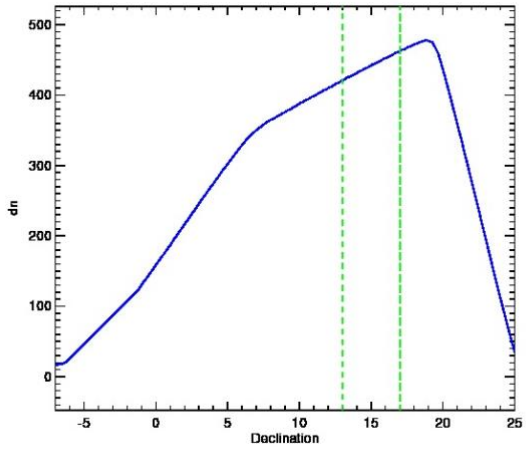

Fig. 5. Sweet spot for SNPP VIIRS band M1 detector 1 shown between the two vertical dash lines within full illumination.

Figure 4, however, also illustrates that the illumination of SD continues on beyond the full illumination due to direct solar exposure. After the instrument passes through the direct solar illumination stage and moves away from the terminator, its flight path continues into the remaining daytime part of the orbit, where the signals from the SD sector registered by the RSBs weaken, as seen in the plot, but clearly remain non-zero. During this remaining part of the daytime orbit, the SV port points away from the Sun into the dark space background, thus the illumination of the SD is not due to any direct solar exposure. The incoming weak signals instead come from light that scatters off Earth's surface and passes through the nadir port to illuminate the SD, as also illustrated in Fig. 3. The green vertical line marks the separation of the two stages of the illumination of SD, first the direct solar exposure stage on the right and later the Earth-scattered light stage on the left. Once the flight goes through the daytime portion and reaches the terminator on the other side, close to declination angle of -180°, the instrument once again enters the night side and the signals coming from the SD sector drops to null.

These persistent non-zero signals in the background during the daytime part of the flight come from light enetring the nadir port that the RSB detectors use to observe and image Earth scenes. In the present study, these signals from the SD sector due to Earth-scattered light during the daytime portion of the flight instead are used to calibrate the RSBs following a similar approach to the official operational method. The caveat for this investigation of the new variant approach is that Earth-scattered light has its own optical or reflectance properties that have not been characterized. Thus the analysis approach for this study necessarily takes on a route different from the operational procedure to characterize these properties before computing the mission-long calibration coefficients, or F-factor, from the variant method.

3. CALIBRATION ALGORITHM OF THE VARIANT METHOD

The formalism of the new variant approach using Earth-scattered light follows the standard methodology that uses full solar illumination [9-11,13] with some modifications.

A. The Formalism

For the Earth-scattered light approach, the luminosity from the SD, $L_{SD}(\lambda)$, for a particular wavelength λ at a given time can be described as

$$L_{SD}(\lambda) = I_{Sun}(\lambda) \cdot \cos(\theta_{SD}) \cdot h(\lambda) \cdot C_{Scat} / d_{ES}^2 , \quad (1)$$

where $I_{Sun}(\lambda)$ is the solar irradiance per unit area on surface normal to the incident light at the distance of one Astronomical Unit (AU), θ_{SD} is the solar-zenith angle of the incident light to the SD, $h(\lambda)$ is the SD degradation (or H-factor) as measured by the SDSM, C_{Scat} is the characterizing function accounting for the reflectance and solar angle dependence associated with the Earth-scattered light, and d_{ES} is the Earth-Sun distance in AU at the time of measurement.

The characterizing function C_{Scat} is akin to the product, in the standard methodology using the data in the sweet spot, of the bidirectional reflectance factor (BRF) of the SD with the VF of the attenuation screen, which is dubbed as the BVP function [20]. The C_{Scat} or the BVP in either methodology is a necessary characterization of any optical effects of the light reaching the SD. In the new variant approach, the light reflected off Earth's surface will have its own unique C_{Scat}, characterizing properties such as the reflectance of Earth's surface or geometrical optics effects associated with viewing geometry.

Given that the Earth-scattered light signals registered by the RSB detectors are faint, typically two orders of magnitude lower than the signals from the full-solar illumination stage, the integrated luminosity, $\Lambda SD(\lambda)$, as

$$\Lambda_{SD}(\lambda) = \int L_{SD}(\lambda, t) dt , \quad (2)$$

is used instead of $L_{SD}(\lambda)$. Specifically for this analysis, each single orbit serves as the basic unit of time interval to carry out the integration, shown in Fig. 4 to the left of the vertical dotted line starting at -7° declination within each orbit, to obtain a single unit of luminosity $\Lambda_{SD}(\lambda)$. This orbit-integrated luminosity provides stronger signals and less noise.

With the orbit-integrated luminosity $\Lambda_{SD}(\lambda)$, the new F-factor f, following effectively the identical calculation to the standard approach, is related to all inputs as

$$f(B,D,M,G) = RVS_{B,SD} \cdot \int RSR_B(\lambda) \cdot \Lambda_{SD}(\lambda) \cdot d\lambda \Big/ \left[\sum_{S,F} \sum_i c_i(B,D,M,G) \cdot dn(B,D,F,S)^i \cdot \int RSR_B(\lambda) \cdot d\lambda \right] \quad (3)$$

where B is band, D is detector, M is the mirror of the half-angle mirror (HAM) that has scan-dependence, G is the gain status of high or low, the outer summation at the denominator is over scan S, in which the mirror side of the HAM is M and the gain status of band B is G, and over frame F, the inner summation is over the prelaunch coefficients c_i relating

instrument response to radiance with the index going from 0 to 2, dn(B,D,F,S) is the digital count signal for the four specified setting, $RSR_B(\lambda)$ is the relative spectral response (RSR) of band B at wavelength λ, and $RVS_{B,SD}$ is the response-versus-scan angle (RVS) effect of the scan mirror for band B in the view direction toward the SD. For the present study, the inclusion of the RVS effect of the scan mirror is not strictly necessary since it is normalized at the SD angle of incidence (AOI).

This formalism sets up the theoretical foundation for the variant approach. In reality, unlike in the operational approach where all inputs are measured, characterized or derived, the Earth-based luminosity as described by Eqn. (1) cannot be directly computed because of unknown effects such as those associated with Earth's reflectance property and the SD reflectance at a different angle of incidence. Specifically, C_{Scat} characterization function in Eqn. (1) is not an a priori known function, and thus the luminosity must be computed or obtained via a different route.

B. The Algorithm

The purported luminosity as described in Eqn. (1), the actual amount of light from the SD reaching the RSB, cannot directly be computed because the C_{Scat} function is an a priori unknown. Instead, this analysis explores Eqn (3) in a step-by-step build up of successively corrected mission-long intermediate F-factor functions to arrive at the new F-factor of the variant method. All known and quantifiable effects are first corrected until the final step where the C_{Scat} function can be cleanly fitted, extracted and finally removed from the new mission-long F-factor. It is noted that these functions are not normalized, and for clarity they are denoted in lower case letter such as f_n.

The first step of this build up is the "F_1-factor" function f_1, the part of the F-factor in Eqn. (1), corresponding to the instrument signal apart from a constant normalization, shown as

$$f_1(B,D,M,G) = 1/\left[\sum_{S,F}\sum_i c_i(B,D,M,G)\cdot\delta(M,M_S)\cdot\delta(G,G_S)dn(B,D,F,S)^i\right] \quad (4)$$

For consistency with the aforementioned one-orbit integration of luminosity aforementioned, the instrumental signal is summed over one orbit to a single instance of f_1. As already previously noted, the inclusion of the RVS effect is not necessary as it only amounts to an issue of normalization for SNPP VIIRS. An example result of the summed instrument signals for band M1 detector 1 is shown in Fig. 6 in magenta, the top curve of the three, for all of f_1 through out the mission. This function does not correspond to the luminosity of Eqn. (1) or (2) since the instrument-summed signals contain all associated effects such as SD degradation, which ultimately need to be removed. It simply serves as a starting point for this analysis, whereby such effects will be removed.

The f_1 function is first corrected for the Earth-Sun distance leading to the "F_2-factor" function f_2 as

$$f_2(B,D,M,G) = \frac{f_1(B,D,M,G)}{d_{ES}^2}. \quad (5)$$

The blue colored curve in Fig. 6, the middle curve of the three, shows the corresponding band M1 detector 1 mission-long f_2 result, which is the summed instrument signals per orbit corrected for Earth-Sun distance. It can be seen that the distance-correction makes a small adjustment from the instrument-summed signals (top curve).

The f_2 function is further corrected for the degradation of the SD, $h(\lambda_B)$, leading to "F_3-factor" function f_3 as

$$f_3(B,D,M,G) = f_2(B,D,M,G)\cdot h(\lambda_B). \quad (6)$$

The SD degradation, or H-factor, is directly taken from the on-orbit characterization result as described by Sun and Wang [14]. Figure 6 shows the corresponding mission-long f_3 result for band 1 detector 1 in the cyan colored curve, the lowest curve of the three. It can be seen that the degradation of the SD is the dominant effect impacting the instrument signals, and its removal leads to a long-term trend (cyan) that is much more gentle for SNPP VIIRS M1.

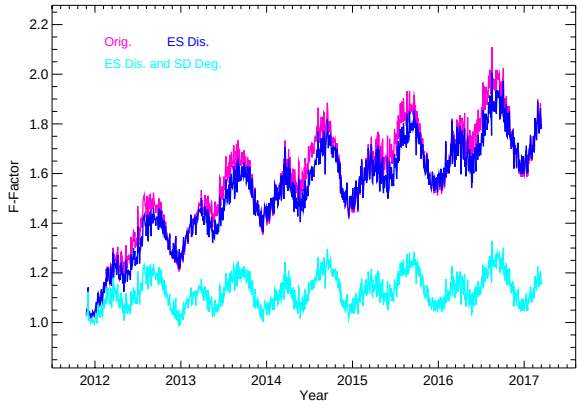

Fig. 6. SNPP VIIRS band M1 detector 1 high gain HAM side 1 F-Factor: Magenta curve is without any correction, f_1; Blue curve is Sun-Earth distance effect corrected, f_2; Cyan curve is corrected for Sun-Earth distance and SD degradation effects.

The mission-long f_3 essentially is the F-factor embedded with C_{Scat} along with other factors. Its underlying long-term pattern reflects the gain change of the RSB performance, or F-factor, and is expected to match the standard F-factor. Its short-term pattern, specifically that of the yearly repetition, is mostly the behavior of C_{Scat} that reflects the combined effect of the Earth's reflectance plus the solar angle dependence as previously stated. Similar to the BVP from the standard operational procedure [13], C_{Scat} is a function depending on the optical property of light reaching the SD and viewing geometry that follow the yearly cycle as the instrument orbits around the Sun.

The final step, the f_4 function, is arrived at via the removal of the short-term yearly pattern via a characterizing function $\Gamma_{B,D,M,G}$

$$f_4(B,D,M,G) = f_3(B,D,M,G)/\Gamma_{B,D,M,G}, \quad (7)$$

where $\Gamma_{B,D,M,G}$ characterizes the following part in Eqn. (1),

$$\Gamma_{B,D,M,G} = \frac{\int RSR_B(\lambda)\cdot d\lambda}{\int RSR_B(\lambda)\cdot\Lambda_{SD}(\lambda)\cdot d\lambda}. \quad (8)$$

The expression shown above in Eqn. (8) connects the yearly modulation to the combined effect of RSR and luminosity Λ_{SD}, the latter of which embeds the C_{Scat} function shown in Eqn. (1). The derivation of the yearly modulation, however, cannot and will not directly go through Eqn. (8). Instead, a fitting scheme to the mission-long f_3 is adopted to extract the function empirically. The derived f_4, after removing for the yearly modulation, then will arrive at the new variant F-factor corresponding to Eqn. (3) for the entire mission, i.e.,

$$f(B,D,M,G) = f_4(B,D,M,G). \quad (9)$$

The extraction of the yearly modulation function from f_3 is achieved through a straightforward fitting of a three-year period first to a quadratic baseline function. The three-year period from the beginning of 2014 through the end of 2017 is selected for this purpose. Figure 7

shows for band M1 detector 1 the three-year f_3 F-factor pattern (in magenta curve) and its quadratic baseline fit (in blue line). The fitting result demonstrates for the three-year period a change of about 30% for the performance of band M1 detector 1.

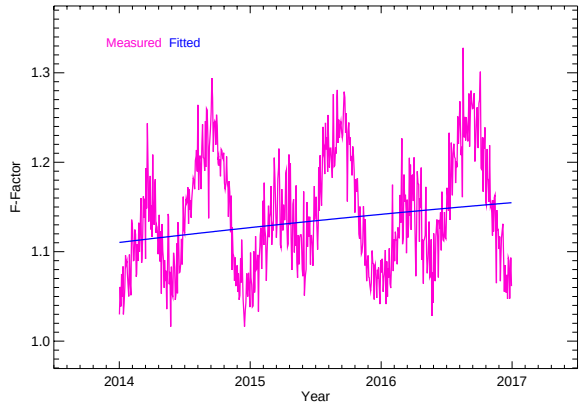

Fig. 7. SNPP VIIRS band M1 detector 1 high gain HAM side 1 F-factor: Magenta curve is Sun-Earth distance and SD degradation effects corrected, f_3; Blue curve is quadratic form fitted to the measured data.

The extraction of the yearly modulation needs first to be separated from the underlying changing trend attributed to the changing RSB performance. For this purpose, a ratio is computed for each f_3 data point, for the three-year period in Fig. 8, over the fitted value. The result of each year is overlaid into a one-year interval to build up a measured value of the yearly modulation, as shown in magenta square symbols in Fig. 8.

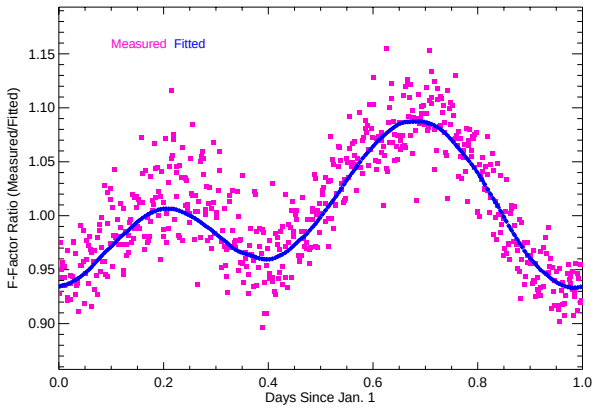

Fig. 8. Seasonal oscillation effects in SNPP band M1 detector 1 high gain HAM side 1 F-factor, f_3; Magenta points are measured value as ratio; Blue curve is the fitted result.

The modulation is assumed to remain an invariant function from one year to the next, and therefore the characterization only needs to be performed once. While the associated properties of Earth's surface possibly can change slowly over time scales of many years, for example due to some permanent changing conditions of Earth's surface, it suffices for this analysis to assume the multi-year constancy of the yearly modulation over the mission of the SNPP VIIRS.

The fitted yearly modulation function is shown in Fig. 8 in the blue curve for band M1 detector 1. It can be seen that the underlying rising trend has been removed, and the value at the beginning of the modulation matches that at the end. The double-peak feature is apparent, with each peak occupying approximately one-half of a year. This fitted modulation function is applied to all years to remove the yearly modulation.

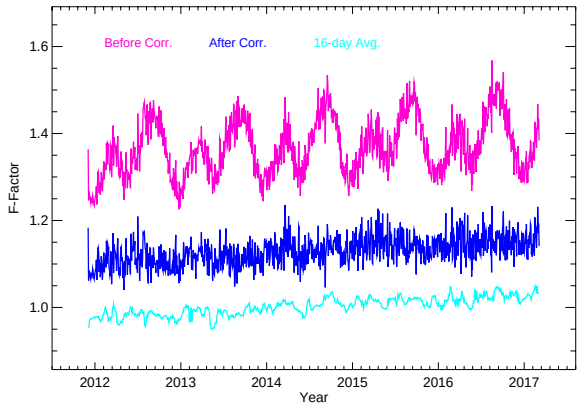

Fig. 9. SNPP VIIRS band M1 detector 1 high gain HAM side 1: Magenta is corrected for the Sun–Earth distance and SD degradation effects, f_3; Blue curve is seasonal oscillation due to all other mechanisms removed, f_4; Cyan curve is result from 16-day average.

In Fig. 9, the three stages of the analysis result are shown for band M1 detector 1, from before the removal of the yearly modulation to the final 16-day average result. The three curves are also purposely offset in the plot for clarity of illustration. The magenta curve is the original f_3 function also shown in Fig. 6 that includes the yearly modulation. The blue curve represents the final F-factor result f_4, plotted for every orbit, after the removal of the yearly modulation. The mission-long F-factor result for band M1 detector 1 shows a steady uptrend leading to an overall change of about 8%. The stable trending without obvious yearly modulating pattern demonstrates that the fitted modulation function indeed is applicable throughout the entire mission as a multi-year invariant.

A 16-day average of the orbit-based F-factor result can be further taken. Because the SNPP satellite follows a 16-day repeat-cycle, each 16-day interval represents a logical unit of data in which a single averaged result can be computed. The 16-day average result for band M1 detector 1 is shown in Fig. 9 as the cyan curve at the bottom, and the noise in the trend has been significantly reduced down to a 2% variation from the ~5% variation prior to the 16-day averaging.

The analysis for all other RSBs follows identical procedure as described above. The fitted modulation functions for the nine RSBs of wavelength 865 nm and shorter are shown in Fig. 10. The same three-year time period from January 1, 2014 to January 1, 2017 is used for the f_3 function of each RSB to derive the corresponding modulation function. For bands M6, M7, and I2, their f_3 function increases with time more dramatically than other shorter wavelength bands such as band M1, especially in early mission. However, in the selected three-year time period, the f_3 functions of these bands remain sufficiently stable, apart the annual oscillations, to allow a quadratic fitting. It can be seen that the modulation functions for different wavelengths are successful and

show very similar yearly pattern, yet clearly differentiate among different bands, demonstrating wavelength-dependency. As these modulation functions capture the yearly surface reflectance of Earth at different spectral regions, this result showing slightly different behavior at different wavelengths is itself of scientific interest. The double peak reflects the yearly changes in reflectance of the entire surface of Earth, with the southern hemisphere dominating the first half of the year and the northern hemisphere dominating the second half of the year as each half goes through its summer period. The solar angle, which follows a yearly cycle, may also impart some non-negligible impact to the shaping of the modulation functions. The pattern of this yearly modulation is entirely different from that of solar-based or lunar-based calibration analysis, and its characterization is necessary but only needs to be done successfully once.

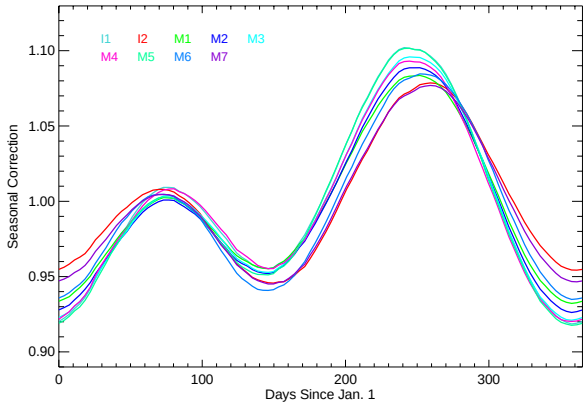

Fig. 10. Seasonal oscillation due to various effects in SNPP band M1 correction functions for seasonal oscillations for SNPP VIIRS visible bands.

Due primarily to much lower signals as well as other miscellaneous issues, bands I3, M8 and other RSBs of longer wavelength bands are not currently analyzed. The analysis of these other bands using Earth-scattered light will require further fine-tuning and a different analysis route that are more appropriately allotted to a different study. It is also found that the shortwave infrared (SWIR) bands have different issues and therefore are not presented in this work.

4. RESULTS AND DISCUSSION

The new mission-long F-factor result using Earth-scattered light for moderate-resolution RSBs up to band M7 (862 nm) is shown in Fig. 11. For each curve, the yearly modulation has been removed and the 16-day average has been taken. It can be seen that all trends show a very consistent 2% variation over the entire mission, indicating that the stability of this orbit-integrated analysis of Earth scattered-light in its present form is about 2%, which is an order of magnitude larger than that of direct illumination using the "sweet spot." The larger uncertainty in the F-factors derived from the Earth-scattered light is mainly induced by the Earth surface temporal variation such as weather changes, as well as the smaller signal to noise ratio (SNR) due to the much smaller instrument response. The SNR for Earth-scattered light cannot be directly derived due to the large noise in signals, but can be derived from the SD data for entire dynamic range from the direct solar illumination range as shown in Fig. 5. However a detailed analysis of the SNR using the SD data is a full analysis of its own and beyond the scope of this paper. Apart from this 2% variability, the analysis demonstrates consistent results for all RSBs shown. The underlying trend over the long-term is otherwise smooth showing no discontinuity or anomaly.

The dependence on band or wavelength for the new F-factor is as expected, showing the general result that the longer wavelength bands have a greater change in F-factor, or greater performance degradation. Band M7 (triangle symbols) and band I2 (diagonal cross symbols) at 862 nm, the two RSBs of longest wavelength among all RSBs shown, show the greatest change over the past five years at about 60% overall, in particular up to 40% during the first year. Bands M6 (circle symbols) and M5 (square symbols), next in rank of wavelength at 745 nm and 671 nm, also show significant change at over 10% and the dramatic first year rise. The four shortest wavelength RSBs, bands M1 through M4, have changed less than 10%. It is already known that band M1 is not the RSB with the smallest F-factor change, and bands M3 and M4 instead are the two bands with the least change [13]. The new F-factor result here also reproduces that result. For all RSBs shown, the trend becomes gentle and almost linear after year 2014.

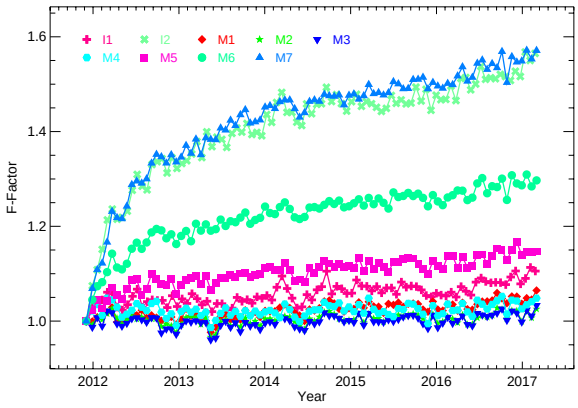

Fig. 11. SNPP VIIRS visible bands F-Factors derived from the SD observations during the periods when the SD is illuminated by the light coming through the nadir port scattered off the Earth's surface.

Figure 12 shows the comparison of the new F-factor result (symbols) for moderate-resolution bands M1–M7 with the standard F-factor (solid lines) result that is computed using full solar illumination. The standard F-factor shown here is taken from the calculation as described by Sun and Wang [13] and has a variation on the level of 0.2%. The two datasets are normalized by matching the respective average of the first half-year of F-factor results. The results for bands I1 and I2 are not shown for the purpose of illustrating more clearly the agreement between the new and the standard results for moderate bands, especially for band M7 whose change is the most dramatic. Otherwise they illustrate the same level of agreement as the moderate band results.

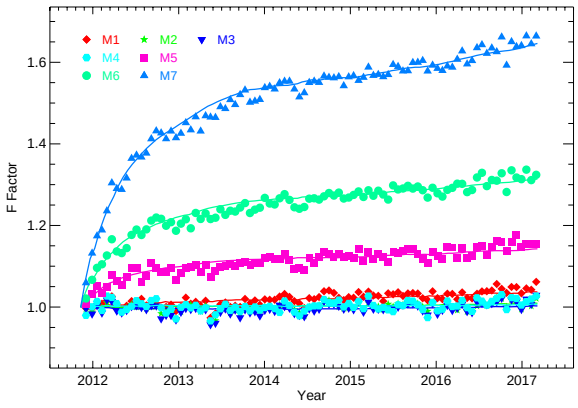

Fig. 12. SNPP VIIRS visible bands F-factors derived from the SD observations: Symbols represent scattered light; Solid lines represent "sweet spot" in the direct solar illumination region.

It is seen that the long-term trend of both the new and the standard sets agree very well over the entire mission for all bands from band M1 to M7. Even for band M7 that has the most dramatic change at about 60%, the new result nevertheless matches the standard result with the same level of agreement as all other RSBs, within the 2% variation, over the entire mission including the early period where the dramatic rise occurs. This demonstrates that the Earth-scattered light signals as registered by the RSBs accurately reflect the performance of the SD reflectance and the gain change of the RSB detectors. Furthermore, this analysis correctly isolates the mission-long F-factor result to capture the correct performance of the RSBs throughout their degradation.

5. GENERAL DISCUSSION

The new variant method has been shown to be viable, but one obvious improvement to the analysis and to make it even more comparable to the standard procedure would be to reduce its uncertainly from the current level of about 2%. There remain some possible nuances in the data not necessarily captured by the orbit-summed signal analysis. For example, navigational or orbital variation can possibly be a factor since the variant method relies on the continual coverage over the entire globe, and therefore can be sensitive to navigational inaccuracy than the operational method that relies only on a short interval of time specific to the Sun view from the SD port. Although to bring down to the 0.2% stability as already achieved in Sun and Wang [13] for the operational procedure seems a serious challenge, achieving a 1% variation is a distinct possibility that can make the variant approach more attractive. Given that the result of the variant approach well match that of the standard approach, a well-constructed fitting scheme can also be implemented to extract the calibration result baseline. Nevertheless, the result of this study shows that the variant method can already be used as a tool for monitoring the standard F-factor result throughout the mission.

One relevant and interesting issue, as mentioned previously, to bring to attention is the "SD degradation nonuniformity (SDDNU) effect" [26], or the non-ideal anisotropic behavior in the degradation of the SD, that causes RSB calibration error. This is because the operational methodology assumes the SD degradation rates at outgoing angle from SD to the RSB and that from the SD to the SDSM to be the same, and therefore the SD degradation measured by the SDSM can be used for RSB calibration. This is in fact an erroneous assumption. This RSB calibration error in SNPP VIIRS and its mitigation has already been addressed by Sun and Wang [29, 30] using a "Hybrid-Method" scheme that mixes in lunar calibration results as mitigation. The solution for the twins MODIS for their affected RSBs is achieved by Sun et al. [27, 28] by abandoning the operational method using the SD and opting to use earth sites for an alternative approach leading to MODIS Collection 6. For the variant approach, the SDDNU effect certainly also will manifest, but in this case it is due to the incident angle, not the outgoing angle, with respect to the SD being different. The light impinging on the SD in the variant method comes through the nadir port, which is different from the operational method where the direction of light is from the SV port to the SD. Therefore, some deviations between the F-factors of the variant approach and the standard approach due to the SDDNU effect potentially can be observed, in particular, for short wavelength bands M1 through M4. Figure 13 shows the F-factors for bands M1-M4 with much smaller scale to demonstrate the SDDNU effect. The RSRs of the short wavelength bands, especially band M1, are known to have some changes during early mission. Thus, data before July 1, 2013 are not included. It can be seen that the two sets of F-factors for each of the four bands diverge slowly with time. The divergence is also band dependent. Over about four years, the divergence is seen to be 1% to 2% for the four bands and the largest divergence appears to be for band M1. Since the directions of incidence on the SD for light from the SD port and nadir are very different, the divergence can be attributed to the result of the SDDNU [26]. The F-factors derived from the new method increase faster with time than those from the standard approach using the data in the "sweet spot". It is known that the F-factors derived from the lunar calibration increase with time faster than those derived from standard SD calibration, and also have more accurate and reliable long-term tread [29]. The F-factors derived with new method are closer to those derived from lunar calibration and well reflect the discrepancy with the standard result due to SDDNU effect. Therefore, the new F-factors may have better long-term accuracy than the standard SD F-factors even though they are noisier in short-term.

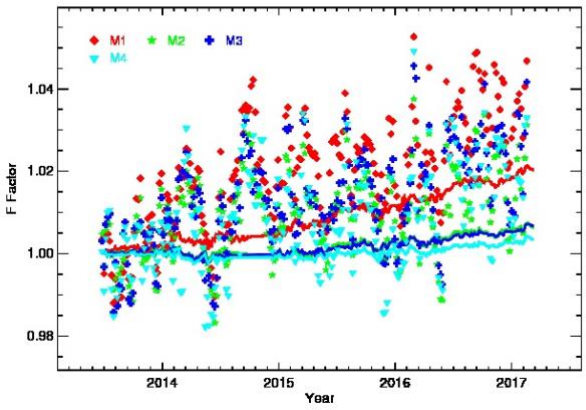

Fig. 13. SNPP VIIRS bands M1-M4 F-factors: Symbols represent scattered light; Solid lines represent "sweet spot".

Because the SD does not have ideal reflectance behavior, this difference in the incident angle is not trivial. The differences in the calculated F-factors from these two approaches are expected and can provide useful quantitative information about the properties of the SD. Provided that SNPP VIIRS can continue to operate for many more years

beyond the seven-year designed lifetime, continual monitoring of the F-factor of the variant method and the operational method eventually is expected to observe the difference caused by the SDNDU effect.

Beyond the new methodology itself, also demonstrated by this investigation is some flexibility in the use of the SD that can enable different considerations for future developments. The variant method demonstrates that a more simplified framework is possible, and it may be possible to consider moving away from the solar-illumination approach or re-orienting the SD for an alternative calibration scheme. New considerations as such potentially can lead to the improvement of the SD degradation treatment or the on-orbit RSB calibration. Although the experience from the twin MODIS and SNPP VIIRS has clearly pointed to the need to improve the current official on-orbit calibration scheme using the SD, the current state of on-orbit RSB calibration nevertheless remains with the use of the SD. Any improved method working within the framework of the SD-based calibration can therefore be highly beneficial going forward. One additional message not to be lost is that similar considerations affect other sensors utilizing a similar diffuser-based calibration scheme.

An earlier effort by Angal et al. [31] has applied a similar approach to both Terra and Aqua MODIS, demonstrating the potential of the variant method to MODIS and other sensors. Although the preliminary result of twin MODIS from that study illustrates up a significant 40% modulation not having accounted for various effects including the removal of the yearly effect associated with the Earth scattered light, its mission-long result exhibited a recognizable trend. Given that MODIS and VIIRS have very similar instrument layout designs, in particular, with both using a SD made of Spectralon in an effectively identical on-orbit RSB calibration strategy, the successful analysis approach demonstrated here should be applicable to MODIS. For MODIS in particular, this variant method is a tantalizing alternative. Had the SD door of Terra MODIS completely failed without being able to be reopened again in the 2007 SD door anomaly [3], thus rendering the operational RSB calibration methodology unusable, this variant method using the scattered light through the nadir port could have been explored as a viable replacement. Although Terra MODIS is currently operating with the SD door in the permanently open position, Aqua MODIS is still operating under a regular open/close operation of the SD door for RSB calibration thus making a similar SD door anomaly a potential concern. In cases as such, the variant method would be an invaluable backup to the standard approach.

The new variant approach in fact is expected to reveal the most interesting result from the SDDNU effect in Terra MODIS since it has the largest SD on-orbit degradation and calibration error among all three sensors [27-29]. Not only is Terra MODIS an older instrument reaching its eighteenth year, it has also been the most exposed to solar radiation especially since the SD door anomaly in 2007 that left the SD door permanently open [3]. On the other hand, examination into Aqua MODIS shows that its SD has with the weakest change in its reflectance [3,4,26] among the three legacy sensors, presumably due to the controlled SD door operation that has prevented excessive solar exposure and space environment contamination. If the application of the variant approach to Terra MODIS and Aqua MODIS indeed demonstrates different results from the standard procedure, it is expected that Terra MODIS and Aqua MODIS will exhibit different levels of differences, that Terra MODIS should exhibit the most clear and significant difference.

Overall, the value of this new consideration is not necessarily about having a new official approach, but definitely it is a useful complementary approach to gain more information and insights, in particular, on the performance of the SD and the standard calibration approach. As the current on-orbit RSB calibration is solely reliant on the SD, and furthermore considering potential complications such as the SDDNU effect, it is not only beneficial but actually of high importance to continue to examine the SD-based calibration methodology in order to prepare for remedy when further complications arise. Although the SDDNU effect itself has been mitigated by the "Hybrid-Method", the effect itself as a complication of the SD reflectance property should continue to be examined. Such studies indeed are difficult since SNPP VIIRS is not equipped for additional on-orbit activities. However, this work shows that it is possible to investigate SD-based calibration methodology under a different framework. The result, as shown in Fig. 13, has already revealed some potential and direct evidence of the different calibration results of the SD-based methodologies. Thus, it is justifying that the standard result as well as the performance of the SD need to be examined.

A different issue of lesser importance is that the illumination coming through the nadir port is significantly weaker than the full solar illumination. Nevertheless the linear regime of the dynamic range is a well established issue, and the Earth scattered light well falls within this range. Therefore, the result of the variant method is expected to match that of the standard method, as is shown by the presented result...

One final point to state is that it is not necessary to refer to these special panels as "solar diffuser" but simply as diffuser in general. This investigation validates the use of Earth, in addition to the to the already established approaches using the Sun and the Moon, to provide viable sources of illumination.

6. CONCLUSIONS

A methodological variant for the onboard calibration of the RSB has been demonstrated to be viable for SNPP VIIRS. The new approach makes a straightforward adaptation of the current official methodology to include the Earth-scattered light through the nadir-port to be used as the illumination source for the SD. The extracted calibration coefficients using the new variant approach, apart from a 2% variation, show good long-term agreement with the standard result derived from the official approach. Central to the successful extraction of the new RSB calibration coefficients is the construction of the seasonal modulation function associated with the Earth-scattered light. This methodological variant demonstrates a viable new alternative that can also help to gain more insights into the behavior of SD degradation. Lastly, this investigation demonstrates the existence of the flexibility within the general procedure of SD-based calibration that can be explored for future considerations.

Funding Information. National Oceanic and Atmospheric Administration (NOAA) and National Aeronautics and Space Administration (NASA) Joint Polar Satellite System.

Acknowledgment. This work was supported by the Joint Polar Satellite System (JPSS) funding. The views, opinions, and findings contained in this paper are those of the authors and should not be construed as an official NOAA or U.S. Government position, policy, or decision.

References

1. W. L. Barnes and V. V. Salomonson, "MODIS: A global imaging spectroradiometer for the Earth Observing System," Crit. Rev. Opt. Sci. Technol. CR47, 285-307 (1993).
2. B. Guenther, W. Barnes, E. Knight, J. Barker, J. Harnden, R. Weber, M. Roberto, G. Godden, H. Montgomery, and P. Abel, "MODIS Calibration: A brief review of the strategy for the at-launch calibration approach", J of Atmospheric and Oceanic Technology 12, 274-285 (1996).

3. X. Xiong, J. Sun, W. Barnes, V. Salomonson, J. Esposito, H. Erives, and B. Guenther, "Multiyear on-orbit calibration and performance of Terra MODIS reflective solar bands", IEEE Trans. Geosci. Remote Sens. 45, 879-889 (2007).
4. X. Xiong, J. Sun, X. Xie, W. L. Barnes, and V. V. Salomonson, "On-orbit calibration and performance of Aqua MODIS reflective solar bands," IEEE Trans. Geosci. Remote Sens. 48, 535–545 (2010).
5. C. J. Bruegge, A. E. Stiegman, R. A. Rainen and A. W. Springsteen, "use of Spectralon as a diffuse reflectance standard for in-flight calibration of earth-orbiting sensors," Opt. Eng. 32, 805-814 (1993).
6. G. T. Georgiev and J. J. Butler, "Long-term calibration monitoring of Spectralon diffuser BRDF in the air-ultraviolet", Appl. Opt. 46, 7892-7899 (2007).
7. T. Scalione, H. W. Swenson, F. De Luccia, C. Schueler, J. E. Clement, L. Darnton, "Post-CDR NPOESS VIIRS sensor design and performance," Proc SPIE 5234, 144-155 (2004).
8. J. J. Puschell, J. Silny, L. Cook and E. Kim, "Future VIIRS enhancements for the integrated polar-orbiting environmental satellite system," Proc SPIE 7813, 78130B (2016).
9. N. Baker, "Joint Polar Satellite System (JPSS) VIIRS radiometric calibration algorithm theoretical basis document (ATBD)," Goddard Space Flight Center, Greenbelt, Maryland, NASA, May 15, 2013.
10. C. Cao, F. Deluccia, X. Xiong, R. Wolfe, F. Weng, "Early on-orbit performance of the Visible Infrared Imaging Radiometer Suite (VIIRS) onboard the Suomi National Polar-orbiting Partnership (S-NPP) satellite," IEEE Trans. Geosci. Remote Sens. 52, 1142–1156 (2014).
11. X. Xiong, J. Butler, K. Chiang, B. Efremova, J. Fulbright, N. Lei, J. McIntire, H. Oudrari, J. Sun, Z. Wang, "VIIRS on-orbit calibration methodology and performance," J. Geophys. Res. Atmos. 119, 5065–5078 (2014).
12. J. C. Cardema, K. Rausch, N. Lei, D. I. Moyer, F. DeLuccia, Operational calibration of VIIRS reflective solar band sensor data records. Proc. SPIE 8510, 851019 (2012).
13. J. Sun and M. Wang, "On-orbit calibration of the Visible Infrared Imaging Radiometer Suite reflective solar bands and its challenges using a solar diffuser," Appl. Opt. 54, 7210-7223 (2015).
14. C. Donlon, B. Berruti, A. Buongiorno, M.-H. Ferreira, P. Féménias, J. Frerick, P. Goryl, U. Klein, H. Laur, C. Mavrocordatos, J. Nieke, H. Rebhan, B. Seitz, J. Stroede, R. Sciarra, "The global monitoring for environment and security (GMES) sentinel-3 mission, " Remote Sensing of Environment 120, 37-57 (2012).
15. H. Oudrari, J. McIntire, X. Xiong, J. Butler, Q. Ji, T. Schwarting, S. Lee, and B. Efremova, JPSS-1 VIIRS radiometric characterization and calibration based on pre-launch testing, Remote Sens. 16, 1647 (2016).
16. J. Sun and M. Wang, "Visible Infrared imaging radiometer suite solar diffuser calibration and its challenges using solar diffuser stability monitor", Appl. Opt. 53, 8571-8584 (2014).
17. J. Fulbright, N. Lei, K. Chiang, and X. Xiong, "Characterization and performance of the Suomi-NPP VIIRS solar diffuser stability monitor," Proc. SPIE 8510, 851015 (2012).
18. H. Oudrari, J. McIntire, X. Xiong, J. Butler, S. Lee, N. Lei, T. Schwarting and J. Sun, "Prelaunch radiometric characterization and calibration of the S-NPP VIIRS sensor," IEEE Trans Geosci and Remote Sens. 53, 2195-2210 (2015)
19. J. McIntire, D. Moyer, B. Efremova, H. Oudrari, X. Xiaoxiong, "On-orbit characterization of S-NPP VIIRS transmission functions", IEEE Trans. Geosci. Remote Sens. 53, 2354-2365 (2015).
20. J. Sun and M. Wang, "On-orbit characterization of the VIIRS solar diffuser and solar diffuser screen," Appl. Opt. 54, 236-252 (2015).
21. T. C. Stone and H. H. Kieffer, "Use of the Moon to support on-orbit sensor calibration for climate change measurements," Proc. SPIE 6296, 62960Y-1-9 (2006).
22. J. Sun, X. Xiong, W. L. Barnes, and B. Guenther, "MODIS reflective solar bands on-orbit lunar calibration", IEEE Trans. Geosci. Remote Sens. 43, 2383-2393 (2007).
23. J. Sun, X. Xiong, and J. Butler, "NPP VIIRS on-orbit calibration and characterization using the Moon," Proc. SPIE 8510, 85101I (2012).
24. X. Xiong, J. Sun, J. Fulbright, Z. Wang, and J. Butler, "Lunar calibration and performance for S-NPP VIIRS reflective solar bands", IEEE Trans. Geosci. Remote Sensing. 54, 1052-1061 (2016).
25. J. Sun, X. Xiong, "Solar and lunar observation planning for Earth-observing sensor," Proc. SPIE 8176, 817610 (2011).
26. J. Sun, M. Chu and M. Wang, "Degradation nonuniformity in the solar diffuser bidirectional reflectance distribution function," Appl. Opt. 55, 6001-6016 (2016).
27. J. Sun, X. Xiong, A. Angal, H. Chen, A. Wu, and X. Geng, "Time dependent response versus scan angle for MODIS reflective solar bands," IEEE Trans. Geosci. Remote Sens., 52, 3159-3174 (2014).
28. J. Sun, A. Angal, X. Xiong, H. Chen, X. Geng, A. Wu, T. Choi, and M. Chu, "MODIS RSB calibration improvements in Collection 6", Proc. SPIE 8528, 85280N (2012).
29. J. Sun and M. Wang, "Radiometric calibration of the visible infrared imaging radiometer suite reflective solar bands with robust characterizations and hybrid calibration coefficients," Appl. Opt., 54, 9331-9342 (2015).
30. J. Sun and M. Wang, "VIIRS reflective solar bands calibration progress and its impact on ocean color products", Remote Sens. 8, 194 (2016).
31. A. Angal, X. Xiong, X. Geng, and J. Sun, "Monitoring the Terra and Aqua MODIS RSB calibration using scattered light from the nadir-port ", Proc. SPIE 9218, 92181J (2014).